

Molecular Physics

An International Journal at the Interface Between Chemistry and Physics

ISSN: (Print) (Online) Journal homepage: <https://www.tandfonline.com/loi/tmph20>


Characterisation of the first electronically excited state of protonated acetylene $C_2H_3^+$ by coincident imaging photoelectron spectroscopy

Gustavo A. Garcia , Jean-Christophe Loison , Fabian Holzmeier , Bérenger Gans , Christian Alcaraz , Laurent Nahon , Xiangkun Wu , Xiaoguo Zhou , Andras Bodi & Patrick Hemberger


To cite this article: Gustavo A. Garcia , Jean-Christophe Loison , Fabian Holzmeier , Bérenger Gans , Christian Alcaraz , Laurent Nahon , Xiangkun Wu , Xiaoguo Zhou , Andras Bodi & Patrick Hemberger (2021) Characterisation of the first electronically excited state of protonated acetylene $C_2H_3^+$ by coincident imaging photoelectron spectroscopy, Molecular Physics, 119:1-2, e1825851, DOI: [10.1080/00268976.2020.1825851](https://doi.org/10.1080/00268976.2020.1825851)



To link to this article: <https://doi.org/10.1080/00268976.2020.1825851>

 View supplementary material 

 Published online: 29 Sep 2020.





 Submit your article to this journal 

 Article views: 82

 View related articles 

 View Crossmark data 

Characterisation of the first electronically excited state of protonated acetylene $C_2H_3^+$ by coincident imaging photoelectron spectroscopy

Gustavo A. Garcia ^a, Jean-Christophe Loison ^b, Fabian Holzmeier ^c, Bérenger Gans ^d, Christian Alcaraz ^e, Laurent Nahon ^a, Xiangkun Wu ^{f,g}, Xiaoguo Zhou ^f, Andras Bodi ^g and Patrick Hemberger ^g

^aSynchrotron SOLEIL, L'Orme des Merisiers, Cedex, France; ^bInstitut des Sciences Moléculaires, UMR 5255 CNRS - Université de Bordeaux, Cedex, France; ^cInstitute of Physical and Theoretical Chemistry, University of Würzburg, Würzburg, Germany; ^dInstitut des Sciences Moléculaires d'Orsay, CNRS, Université Paris-Saclay, Orsay, France; ^eInstitut de Chimie Physique, CNRS, Université Paris-Saclay, Orsay, France; ^fHefei National Laboratory for Physical Sciences at the Microscale, Department of Chemical Physics, University of Science and Technology of China, Hefei, Peoples Republic of China; ^gLaboratory for Synchrotron Radiation and Femtochemistry, Paul Scherrer Institute, Villigen, Switzerland

ABSTRACT

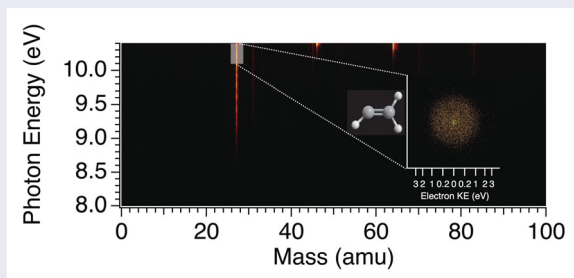
We present a combined experimental and theoretical study of the threshold photoelectron spectroscopy of the vinyl radical encompassing the first triplet excited state of the vinyl cation. The radicals were produced in a flow-tube reactor by hydrogen abstraction of C_2H_4 and CH_4 using fluorine atoms generated in a microwave discharge. Vinyl was ionised with synchrotron vacuum ultraviolet radiation. A double imaging coincidence setup was used to record the threshold photoelectron spectrum. The experimental and simulated spectra show a marked adiabatic transition to the $\tilde{a}^+ \ ^3A''$ state with a short vibrational progression dominated by the $C = C$ stretching mode. The adiabatic ionisation energy to this state is measured precisely at 10.747 ± 0.008 eV. In combination with the adiabatic ionisation energy to the $\tilde{X}^+ \ ^1A_1$ state from the Active Thermochemical Tables (ATcT), we find a singlet–triplet gap of 2.27 ± 0.01 eV (219 ± 1 kJ mol⁻¹). Calculated ionisation energies and Franck–Condon factors for the singlet $\tilde{A}^+ \ ^1A''$ excited state are also given.

ARTICLE HISTORY

Received 30 July 2020
Accepted 10 September 2020

KEYWORDS





Protonated acetylene; vinyl radical; photoelectron spectroscopy; synchrotron




1. Introduction

The vinyl radical, C_2H_3 , is an important reactive intermediate in combustion reactions [1] and plasma processes [2] and is also involved in H-abstraction reactions with polycyclic aromatic hydrocarbons (PAH), [3] which are linked to PAH growth. Besides, both neutral and cation forms are present in low temperature reactions in planetary atmospheres and satellites, [4,5] as well as in dense interstellar clouds, [6,7] where they contribute to the generation of larger organic molecules $C_{n>3}$, and eventually to aerosols [4]. Understanding the cation

spectroscopy is therefore of fundamental importance to model the vinyl photochemistry and reactivity in ultraviolet (UV) and vacuum ultraviolet (VUV) irradiated regions. The vinyl cation, also known as protonated acetylene, can also be formed by ion-molecule reaction between ionised acetylene $C_2H_2^+$ and H_2 in circumstellar and interstellar clouds [8]. However, the first adiabatic ionisation energy of the C_2H_3 radical cannot be measured by single-photon ionisation, due to the large geometry change between the neutral species (C_s symmetry, bent-Y shaped) and the cation (C_{2v}

CONTACT Gustavo A. Garcia  gustavo.garcia@synchrotron-soleil.fr  Synchrotron SOLEIL, L'Orme des Merisiers, Saint Aubin BP 48, F-91192 Gif sur Yvette, Cedex, France; Patrick Hemberger  patrick.hemberger@psi.ch  Laboratory for Synchrotron Radiation and Femtochemistry, Paul Scherrer Institute, 5232 Villigen, Switzerland

 Supplemental data for this article can be accessed here. <https://doi.org/10.1080/00268976.2020.1825851>

symmetry, bridged shaped, see Scheme 1), as recently shown by Wu *et al.*, [9] who attributed the first band of the photoelectron spectrum to several transitions, none of them including the adiabatic one. These findings also revealed large variations of the observed ionisation energy with temperature, since two of the transitions are related to the region of the C_{2v} straight-Y shaped transition state in the neutral—only accessible at high internal energies (*ca.* 0.2 eV)—and to the steeply varying Franck–Condon (FC) factors, putting to rest earlier discrepancies in the apparent ionisation energy values reported in the literature.

To complement previous experimental works in the literature on the photoionisation of C_2H_3 , [9–16] here we will focus on the characterisation of the first electronically excited state of the $C_2H_3^+$. This information is also crucial to chemistry models since internal excitation can have a dramatic effect on the species reactivity [17], more so at low temperatures where quantum effects become dominant. In addition, high resolution photoelectron spectra of excited states of radicals present rare opportunities to benchmark theoretical models through more stringent tests. Indeed, measuring transitions to excited states of the cation is more challenging since they usually overlap with the precursor signal (as is the case in the current work), and often lack fine structure due to the short lifetimes linked to fast internal conversion or dissociative ionisation processes.

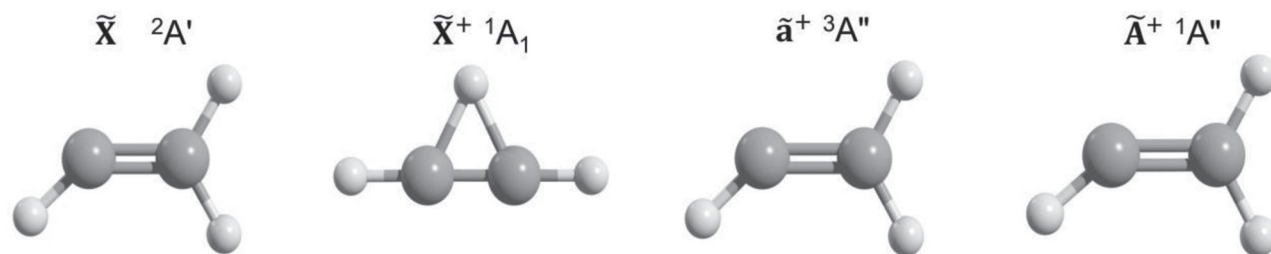
In this work, we have measured the threshold photoelectron spectrum over an energy range encompassing the ground and first electronically excited states of $C_2H_3^+$, by photoionisation of the vinyl radical produced by H abstraction of ethene or by H abstraction of methane and further reactions, and we attribute the observed vibrational structures of the first triplet $^3A''$ state *via* high level *ab initio* calculations and a FC simulation. Moreover, photoelectron spectra have been increasingly used over the past decade as fingerprints of molecular structure in advanced mass spectrometry techniques for *in-situ*, real-time species detection and

quantification in complex gas phase media [18]. Radical species hold the key to understanding the reaction mechanism, for instance, in atmospheric chemistry [19–23] or in more aggressive environments, such as combustion [24–26], pyrolysis [27,28], or catalysis [29]. To unambiguously reveal the mechanism, radicals must be detected isomer-selectively. Photoelectron photoion coincidence (PEPICO) endstations [23,30,31] are routinely used to record photoelectron spectral fingerprints of elusive species to identify them and assign the mass spectrum. They are typically located at third generation synchrotron facilities, such as Soleil, [32] or the Swiss Light Source [33]. In this context, the first photoelectron band is typically used because it is more readily available and does not often lead to fragmentation, increasing the analytical applicability. However, excited states add not only another layer of confidence but also selectivity and sensitivity to the identification, especially in cases where structure is visible, such as in the case of the vinyl radical. There, the energy region of the $^3A''$ cation state may provide a superior fingerprint than that of the 1A_1 state, because of the weak and slowly changing FC factors for transitions to the latter. This adds further motivation to the study of the threshold photoelectron spectrum of vinyl above the 1A_1 cation state.

2. Methodology

2.1. Experimental

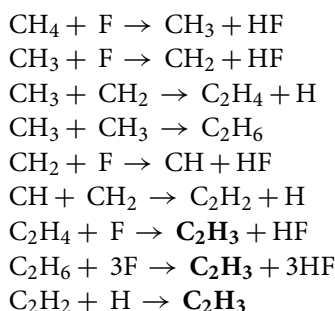
Experiments were performed at the variable polarisation undulator-based beamline DESIRS [32], on the molecular beam endstation SAPHIRS [34]. The radical production scheme and its coupling to the SAPHIRS endstation has been described previously in detail [35]. In this work, F atoms (few 10^{13} atoms cm^{-3}) were produced in a microwave discharge of a 5% mixture of F_2 in He (Air Liquide) and fed into a quartz flow-tube reactor through a sidearm, while the precursor was diluted in He and entered the reactor *via* a moveable injector. The injector-nozzle distance was adjusted to deliver a reaction time of



Scheme 1. Structures of the vinyl radical (\tilde{X}^2A') and three cation states, investigated in this study. While the minimum cation ground state (\tilde{X}^+1A_1) structure is the non-classical bridge shape, both the \tilde{a}^+3A'' and \tilde{A}^+1A'' states are similar to the radical structure (bent-Y shape). This leads to large Franck–Condon factors for both the $\tilde{a}^+3A'' \leftarrow \tilde{X}^2A'$ and $\tilde{A}^+1A'' \leftarrow \tilde{X}^2A'$ origin transitions.

about 1 msec. The total pressure of the flow-tube reactor was maintained at 1–2 Torr. Two precursors were used to produce the C_2H_3 radical, the first and most obvious being ethene (99.95%, Air Liquide) through a single-H abstraction: $C_2H_4 + F \rightarrow C_2H_3 + HF$ ($\Delta_r H^\circ = -109.7$ kJ mol⁻¹ [36]). This reaction was used to obtain the data in the photon energy range 8.0–10.3 eV containing the ground state of the C_{2v} straight-Y and bridge shaped cations.

To avoid saturation by the C_2H_4 precursor above its ionisation energy (10.5 eV), methane (99.95% from Air Liquide, 2.0×10^{14} molecules cm⁻³ diluted in He) was used as precursor for the energy range 10.3–12.0 eV, which may lead to the formation of C_2H_3 through different multistep reaction pathways, for example:



The contents of the flow-tube expanded through a 1 mm Teflon nozzle and traversed a 2 mm Ni skimmer before reaching the interaction region where they were ionised by the vacuum ultraviolet (VUV) synchrotron radiation at the centre of the double imaging photoelectron photoion coincidence (i²PEPICO) spectrometer DELICIOUS-3 [30]. The DESIRS beamline was set to deliver 4×10^{12} photons s⁻¹ with a resolution of 14 meV at 11 eV and linearly polarised light in the detection plane. The high harmonics from the undulator were filtered out by filling a differentially pumped gas cell upstream the monochromator with Ar [37]. The electrons and ions produced were accelerated in opposite directions by a continuous electric field (89 V cm⁻¹ for the C_2H_4 and 36 V cm⁻¹ for the CH_4 precursor) and analysed by a velocity map imaging [38] and a modified Wiley–McLaren momentum imaging device, respectively. The ion momentum imaging device was set to space imaging, where the arrival position on the detector is correlated, for a parent ion, to the location of its formation in the interaction region and to its net velocity along the molecular beam, as described earlier [35]. Under these conditions, the coincidence scheme was used to mass-tag the photoelectron images and to select only neutrals originating directly from the flow-tube reactor, *i.e.* having an additional velocity component along the molecular beam, increasing the signal-to-background

ratio. The ionisation events are further filtered to suppress those that originate too far away from the centre of the interaction region, which improves the ion mass and electron kinetic energy resolution. The filtered photoelectron images were subsequently Abel-inverted [39] to obtain the photoelectron spectrum at each photon energy of the scan, *i.e.* between 8 and 12 eV with 5 meV steps. All the photon energy dependent data have been normalised by the photon flux, as measured with Si photodiode (AXUV, Opto Diode). The photon energy scale has been calibrated with ± 5 meV precision using the 4s' absorption of the Ar in the gas filter [40], and the known ionisation energies of C [41] and C_2H_2 [42].

2.2. Theoretical

Quantum chemical calculations have been performed using the Q-Chem [43] and Gaussian16 [44] suites of programs. Accurate adiabatic ionisation energies for the $\tilde{a}^+ \ ^3A'' \leftarrow \tilde{X} \ ^2A'$ transition were determined utilising CBS-QB3, CBS-APNO, G3, G4, and W1BD composite methods. The geometries and vibrational frequencies were taken from the W1BD calculations [45,46]. Furthermore, optimisation and frequency analysis for the D_0 neutral, the S_1 and T_0 cation states have been performed using the cc-pVTZ and cc-pVQZ basis sets and various flavours of coupled cluster calculations within the frozen-core approximation. The neutral state was addressed in ground-state CCSD calculations as well as using the singlet cation ground state reference and the equation-of-motion electron affinity (EOM-EA-)CCSD approach. The triplet ground state can be calculated directly, as done in the composite method calculations, but the results are more consistent if an approach is chosen that is applicable to the S_1 cation state, as well. Thus, equation-of-motion excitation energy (EOM-EE-)CCSD results are reported for the triplet and the first excited singlet cation states. Combined with an EOM-EA-CCSD neutral energy, this means that ionisation energies to the S_1 and T_0 states are reported based on the fully relaxed spin eigenfunction Hartree–Fock reference wave function of the S_0 cation and EOM-CCSD electron affinity as well as excitation energy calculations. The nuclear geometries were optimised in each energy calculation at the respective level of theory and a frequency analysis was carried out to confirm that minima were found and to include zero-point-energies in the reported adiabatic ionisation energies. The threshold photoelectron spectra have been simulated utilising ezSpectrum [45] and were subsequently convoluted with a Gaussian function (FWHM = 30 meV) to account for the energy resolution of the experiment and the rotational broadening of the

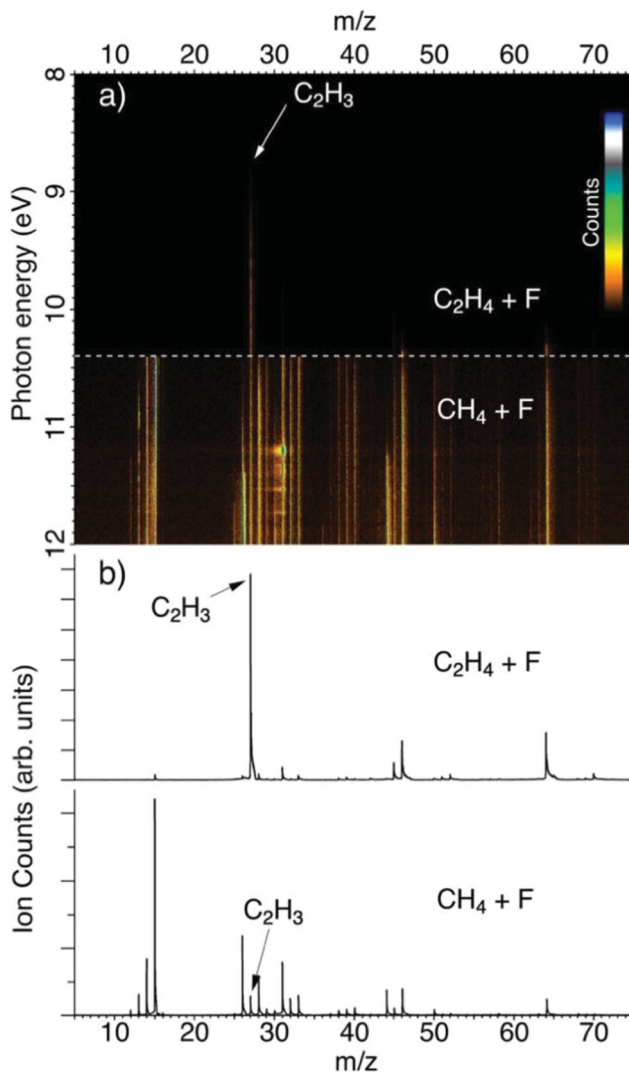


Figure 1. (a) TOF-MS as a function of the photon energy measured using ethene (≤ 10.4 eV, top) and methane (> 10.4 eV, bottom) as precursors. The data have been normalised using the m/z 27 signal and the colormap has been saturated to bring out low intensity details. (b) TOF-MS integrated over the photon energy range corresponding to each precursor (8–10.4 eV for $C_2H_4 + F$ and 10.4–12 eV for $CH_4 + F$).

spectrum. The vibrational modes are numbered according to the Mulliken convention, *i.e.* by dividing them into symmetry blocks and sorting them in descending order according to energy.

3. Results and discussion

Figure 1 shows the time-of-flight (TOF) mass spectra as a function of the photon energy for both methane and ethene precursors. We deliberately added a relatively high concentration of F atoms in the methane experiments to produce $C_2H_{x=1,3,5}$ radicals, which increases the level of

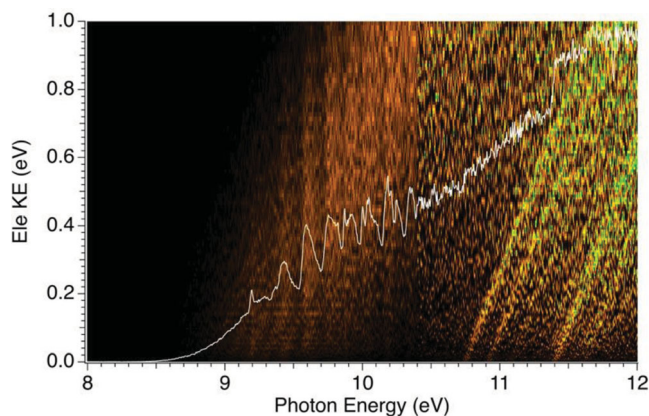


Figure 2. Signal intensity as a function of electron kinetic energy and photon energy for m/z 27. The white line represents the total ion yield. The signal-to-background ratio is markedly lower above 10.4 eV due to the decreasing signal in the m/z 27 channel in the $CH_4 + F$ reaction, with respect to $C_2H_4 + F$.

chemical complexity in the reactor, as seen in the TOF-MS where tens of species are seen, including the products of multiple-H abstractions (CH_2 , CH , and C). In these conditions, the m/z 27 channel corresponding to C_2H_3 amounts to a small fraction of the total signal. In contrast, the TOF of the ethene reaction is much cleaner, because the reactor conditions were set for a single H abstraction, *i.e.* lower F concentration and shorter reaction time, and the m/z 27 channel is dominant.

The number of events as a function of electron kinetic energy and photon energy is depicted as a 2D colormap in Figure 2 for the m/z 27 channel. In this representation, diagonal lines of unity slope $eKE = h\nu - IE_i$, where IE_i is the ionisation energy of a cationic state, correspond to direct ionisation of the i^{th} state, while vertical features correspond to autoionisation resonances that depend on the photon energy, which are also seen as resonant features in the total ion yield (TIY) represented alongside. A number of direct and resonant features are indeed seen in these data and will be further commented on below. The 2D data can be reduced in several ways, and in Figure 3(a), we present the slow photoelectron spectrum (SPES). The method reveals the cationic states by integration along the diagonal lines as previously described [47]:

$$SPES(h\nu) = \int_0^{KE_{\max}} A(h\nu + KE, KE) dKE$$

where A is the 2D matrix in Figure 2, and $KE_{\max} = 0.075$ eV is the integration bandwidth. Under these conditions, the electron energy resolution was measured at 17 meV on the C atom peak obtained within the same scan, leading to a combined electron and photon energy resolution of 23 meV.

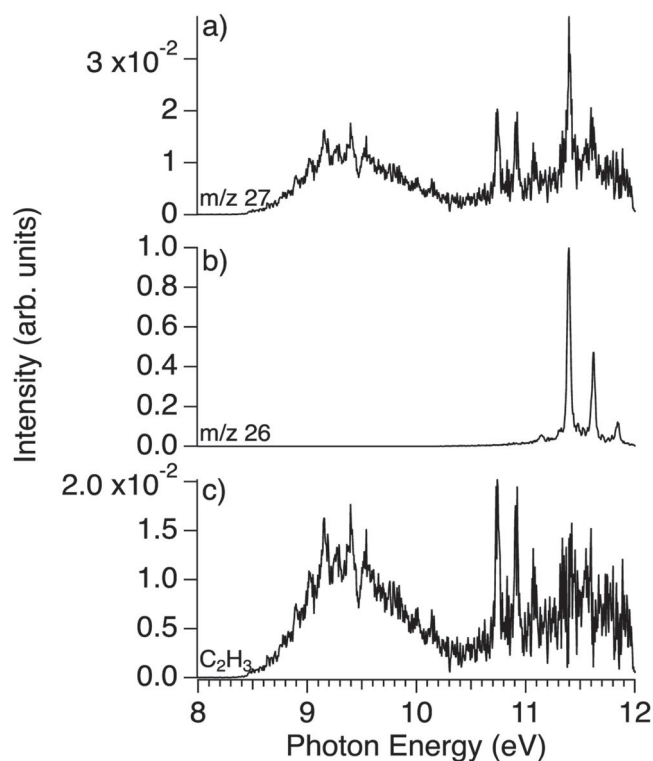


Figure 3. SPES for (a) m/z 27, (b) m/z 26 and (c) C_2H_3 after subtracting the contribution from $H^{13}C \equiv ^{12}CH$ to m/z 27. The three vertical axes have been normalised to the maximum signal of the m/z 26 SPES to show the unfavourable signal ratios.

Also shown in Figure 3(b) is the SPES obtained for the C_2H_2 , m/z 26, which is formed in large quantities in the $CH_4 + F$ reaction (see Section 2.1). The most prominent features in the SPES correspond to the ν_2^+ ($C \equiv C$ stretch) progression in the $\tilde{X}^+ \ ^2\Pi_u$, including a hot band at 11.15 eV from $\tilde{X}^+ \ ^2\Pi_u(\nu_2^+ = 0) \leftarrow \tilde{X} \ ^1\Sigma_g^+(\nu_2 = 1)$. Regrettably, the C_2H_2 signal is nearly 50 times that of C_2H_3 above the acetylene ionisation energy, 11.4 eV. Therefore, as apparent when comparing the spectra in Figure 3(a,b), there is a non-negligible amount of acetylene contaminating the C_2H_3 spectrum due to the 2.2% natural abundance of the $H^{13}C \equiv ^{12}CH$ isotopologue. In Figure 3(c), we have subtracted this contribution, within the limits of the signal-to-background ratio and the slight frequency downshift of the $H^{13}C \equiv ^{12}CH$ isotopologue.

As mentioned in the introduction, Wu *et al.* [9] prepared the vinyl radical in a hot pyrolysis microreactor, and attributed the rising edge of the first band, spanning the 8.2–10.4 eV range, to transitions from the vicinity of the straight-Y geometry, a transition state in the neutral, to the bridged global and straight-Y local minimum of the cation. At slightly higher energies, transitions from the bent-Y neutral minimum to the straight-Y local minimum of the cation may also contribute, but the

FC overlap between the neutral and cation global minima, *i.e.* corresponding to the adiabatic ionisation energy, were found to be negligible. Indeed, the structure of the cationic ground state has been discussed at length in the literature, both experimentally [12,48–53] and theoretically [54–56], with the non-classical bridged form being the most stable one, precluding the direct observation of the adiabatic transition by one photon ionisation from the bent-Y neutral minimum. The energy difference between the classical and non-classical geometries was experimentally estimated at about 0.2 eV [49], but due to the unfavourable FC factors to the non-classical one, the importance of the higher energy straight-Y structure in the FC envelope means that temperature plays an important role in the shape of this band, and hence influences the observed ionisation energy. It is then interesting that the SPES in this region, recorded at room temperature in our flow-tube reactor, is very similar to the one of Wu *et al.* [9], which suggests the presence of the straight-Y neutral in our reactor in comparable amounts to the pyrolysis study, which was performed at 800°C. This is, however, easily explained by the exothermicity of the $C_2H_4 + F$ reaction, since an energy of 1.14 eV will be shared between HF and C_2H_3 . Indeed, although the translational (= rotational) temperature of the flow-tube species is measured *via* ion imaging at around 160 K due to the mild expansion through the nozzle and skimmer, it is common to observe electronically excited species or high energy isomers in our reactor [57,58].

At 10.743 eV, a progression starts with a spacing of 170 meV (1370 cm^{-1}), which is assigned to the $\tilde{a}^+ \ ^3A'' \leftarrow \tilde{X} \ ^2A'$ transition and confirmed by composite methods calculations as summarised in Table 1. The clear vibrational structure speaks for a small change in geometry upon ionisation, which is also confirmed by the FC simulations. The latter were performed using the geometries and force constants from the W1BD calculations. Upon forming the triplet cation state, the electron is removed from the least stable orbital below the Singly Occupied Molecular Orbital [9], (SOMO–1), which has binding character along the $C=C$ bond and, thus, removing an electron elongates this bond in the ionisation process. The FC simulation is depicted in Figure 4 and nicely reproduces the experimental spectrum with the dominating $C=C$ stretching vibration (ν_5) with a calculated vibrational wavenumber of 1330 cm^{-1} . The second peak at 10.91 eV has a smaller contribution of the ν_4 mode and is assigned to the $H-C-H$ bending vibration (scissoring mode) at 1466 cm^{-1} . Overtones and combination bands are responsible for the increased broadening of the progression above 11 eV, but only the ν_4 and ν_5 modes are active upon ionisation into the triplet state. The FC simulation extends to roughly 11.3 eV where the

Table 1. Summary of the experimental and theoretical (including zero-point correction) adiabatic ionisation energies (AIE) in eV for both the $\tilde{a}^+{}^3A''$ and $\tilde{A}^+{}^1A''$ cation states of the vinyl radical, obtained in this work.

Method	AIE($\tilde{a}^+{}^3A''$)	AIE($\tilde{A}^+{}^1A''$)
Experimental: ms-SPES ^a	10.747 ± 0.008	
Theory:		
CBS-QB3	10.79	
CBS-APNO	10.77	
G3	10.76	
G4	10.78	
W1BD	10.74	
EOM-EA/EE-CCSD/cc-pVTZ ^b	10.51	11.31
EOM-EA/EE-CCSD/cc-pVQZ ^b	10.59	11.86
CCSD/cc-pVTZ and EOM-EE-CCSD/cc-pVTZ ^c	10.58	11.37
CCSD/cc-pVQZ and EOM-EE-CCSD/cc-pVQZ ^c	10.65	11.93

^aThe value has been corrected up by the 4 meV Stark shift due to the 35 V cm⁻¹ extraction field.⁵⁹ The statistical error bars include the precision of the energy calibration and the errors from the fit by a Gaussian profile.⁶⁰

^bUsing the singlet cation ground state as reference wave function together with an EOM electron affinity calculation to the neutral ground state \tilde{X}^2A' and an EOM excitation energy calculation to the $\tilde{a}^+{}^3A''$ and $\tilde{A}^+{}^1A''$ cation states.

^cSame as (b) but with an unrestricted CCSD calculation for the neutral \tilde{X}^2A' state.

intensity vanishes. Note that the vibrational structure of the $\tilde{a}^+{}^3A''$ state is similar to the autoionisation structures seen in the 9.4–10.4 eV region (Figure 2), as already noted by Wu *et al.* [9], suggesting that these structures arise from Rydberg states converging to the $\tilde{a}^+{}^3A''$ state which then autoionise towards the $\tilde{X}^+{}^1A_1$ ground cationic state.

Above 11.4 eV, the experimental SPES signal rises again, but, as mentioned above, the signal-to-noise ratio

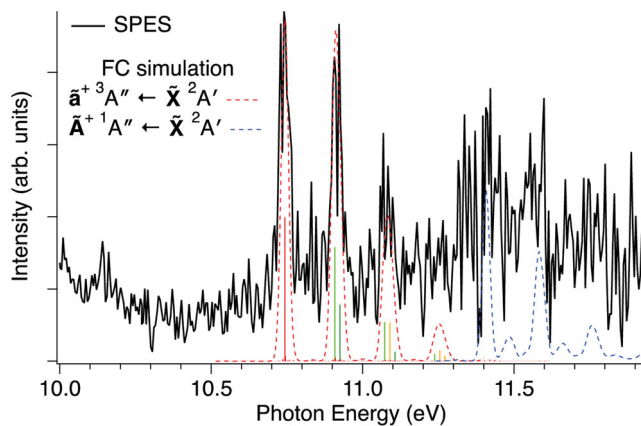


Figure 4. SPES of C₂H₃ (black) in the photon energy region around the first triplet state of the cation. The simulated SPES for the transitions to the triplet $\tilde{a}^+{}^3A''$ (red dashed line) is plotted alongside the FC factors for the C = C stretch (green sticks), HCH bending (forest green sticks) and C = C stretch/HCH bend combination bands (orange sticks). The simulated transition to the singlet $\tilde{A}^+{}^1A''$ state (blue dashed line) is plotted too (see text for details).

deteriorates in this region because of the need to subtract the H¹³C ≡ ¹²CH signal. Nevertheless, in order to evaluate potential contributions from the $\tilde{A}^+{}^1A'' \leftarrow \tilde{X}^2A'$ transition of vinyl, we have carried out additional (equation-of-motion) coupled cluster calculations. The FC simulation of this transition presented in Figure 4 and Figure S1 of the ESI show a similar progression to the one into the $\tilde{a}^+{}^3A''$ ion state, indicative of a small change in geometry upon ionisation with significantly high FC factors. However, a good fit with the features appearing above 11.4 eV could not be achieved. The calculated $\tilde{A}^+{}^1A'' \leftarrow \tilde{X}^2A'$ ionisation energy strongly depends on the basis set with the quadruple- ζ results being ca. 0.55 eV higher than the triple- ζ ones, but are consistent whether a separate CCSD calculation or an electron affinity calculation is used for the neutral (Table 1). Extrapolation to the basis set limit would further increase the $\tilde{A}^+{}^1A'' \leftarrow \tilde{X}^2A'$ ionisation energy. Furthermore, composite methods yield accurate ionisation energies into the $\tilde{a}^+{}^3A''$ state, while coupled cluster EOM approaches underestimate the IE by up to 200 meV. Thus, the CCSD-computed $\tilde{A}^+{}^1A''$ ionisation energy is likely underestimated by more than 0.3 eV using the quadruple- ζ basis, and is likely above 12 eV. The signal at 11.4 eV is probably caused by the imperfect subtraction of the ¹³C component of acetylene or is due to the autoionising Rydberg states converging to the $\tilde{A}^+{}^1A''$ state. The full FC simulation for transitions to the $\tilde{A}^+{}^1A''$ state is shown in Figure S1.

4. Conclusion

We have produced the vinyl radical by two different reactions in a microwave discharge flow-tube and recorded the threshold photoelectron spectroscopy up to a photon energy including the first electronically excited state of the vinyl cation. Adiabatic ionisation energies have been calculated to assist the assignment and to benchmark different theoretical approaches and basis sets, and the FC simulation provides excellent agreement with the experimental spectrum, providing an unambiguous assignment of the $\tilde{a}^+{}^3A''$ band and a precise value for the AIE of this state at 10.747 ± 0.008 eV. Our analysis shows that vibrationally resolved excited state spectra can be used to increase the selectivity, sensitivity and detection capabilities of PEPICO techniques even if the ion ground state does not show a pronounced vibrational structure. Furthermore, by using the enthalpies of formation at 0 K of the bridged-shape C₂H₃⁺ from the Active Thermochemical Tables (ATcT), an AIE of 8.478 ± 0.007 eV is extracted for the $\tilde{X}^+{}^1A_1 \leftarrow \tilde{X}^2A'$ transition, leading to a singlet–triplet gap of 2.27 of ± 0.01 eV (218.9 kJ mol⁻¹)

of the vinyl cation. The transition energy to the first singlet excited state of $C_2H_3^+ \tilde{A}^+ 1A'' \leftarrow \tilde{X}^2A'$ has also been calculated, and extrapolation to the basis set limit would place the AIE 1.3 eV above the triplet state, *i.e.* slightly above 12 eV and outside of the energy range of the present experiment.

Acknowledgements

GAG, BG, JC, FH, CA and LN acknowledge SOLEIL for provision of synchrotron radiation facilities under project number 20140832 and the DESIRS beamline staff for their assistance, in particular J.-F. Gil for his help in the mounting of the reactor radical sources. The authors would also like to thank J. Krüger, A. Röder and A. Lopes for their invaluable help in performing the $CH_4 + F$ experiments. Calculations were carried out at the Paul Scherrer Institute.











Disclosure statement

No potential conflict of interest was reported by the author(s).

Funding

This work received financial support from the French Agence Nationale de la Recherche (ANR) [grant number ANR-12-BS08-0020-02 (project SYNCHROKIN)].

ORCID

Gustavo A. Garcia  <http://orcid.org/0000-0003-2915-2553>
 Jean-Christophe Loison  <http://orcid.org/0000-0001-8063-8685>
 Fabian Holzmeier  <http://orcid.org/0000-0001-8749-5330>
 Bérenger Gans  <http://orcid.org/0000-0001-9658-2436>
 Christian Alcaraz  <http://orcid.org/0000-0002-6816-4664>
 Laurent Nahon  <http://orcid.org/0000-0001-9898-5693>
 Xiangkun Wu  <http://orcid.org/0000-0001-8515-3302>
 Xiaoguo Zhou  <http://orcid.org/0000-0002-0264-0146>
 Andras Bodi  <http://orcid.org/0000-0003-2742-1051>
 Patrick Hemberger  <http://orcid.org/0000-0002-1251-4549>

References

- [1] W.C. Gardiner, Jr, *Gas-Phase Combustion Chemistry* (Springer-Verlag, 2000).
- [2] G.M. Petrov and J.L. Giuliani, *J. Appl. Phys.* **90**, 619 (2001). doi:10.1063/1.1373701
- [3] X.-M. Cao, Z.-R. Li, J.-B. Wang and X.-Y. Li, *Theor. Chem. Acc.* **139**, 3433 (2020).
- [4] P.N. Romani, J. Bishop, B. Bézard and S. Atreya, *Icarus*. **106**, 442 (1993). doi:10.1006/icar.1993.1184
- [5] Y.L. Yung, M. Allen and J.P. Pinto, *Astrophys. J. Supp. S.* **55**, 465 (1984). doi:10.1086/190963
- [6] D. Smith, *Phil. Trans. R. Soc. Lond. A.* **324**, 257 (1988). doi:10.1098/rsta.1988.0016
- [7] E. Herbst and C.M. Leung, *Astrophys. J. Supp. S.* **69**, 271 (1989). doi:10.1086/191314
- [8] A.E. Glassgold, A. Omont and M. Guélin, *Astrophys. J.* **396**, 115 (1992). doi:10.1086/171701
- [9] X. Wu, X. Zhou, P. Hemberger and A. Bodi, *Phys. Chem. Chem. Phys.* **21**, 22238 (2019). doi:10.1039/C9CP04493K
- [10] A.G. Harrison and F.P. Lossing, *J. Am. Chem. Soc.* **82**, 519 (1960). doi:10.1021/ja01488a003
- [11] F.P. Lossing, *Can. J. Chem.* **49**, 357 (1971). doi:10.1139/v71-060
- [12] J. Berkowitz, C.A. Mayhew and B. Rušćić, *J. Chem. Phys.* **88**, 7396 (1988). doi:10.1063/1.454352
- [13] J.A. Blush and P. Chen, *J. Phys. Chem.* **96**, 4138 (1992). doi:10.1021/j100190a004
- [14] I. Fischer, *Int. J. Mass Spectrom.* **216**, 131 (2002). doi:10.1016/S1387-3806(02)00592-4
- [15] J.C. Robinson, N.E. Sveum and D.M. Neumark, *J. Chem. Phys.* **119**, 5311 (2003). doi:10.1063/1.1606440
- [16] J.D. Savee, J.F. Lockyear, S. Borkar, A.J. Eskola, O. Welz, C.A. Taatjes and D.L. Osborn, *J. Chem. Phys.* **139** 056101 (2013). doi:10.1063/1.4817320
- [17] B. Cunha de Miranda, C. Romanzin, S. Chefdeville, V. Vuitton, J. Žabka, M. Poláček and C. Alcaraz, *J. Phys. Chem. A.* **119**, 6082 (2015). doi:10.1021/jp512846v
- [18] T. Baer and R.P. Tuckett, *Phys. Chem. Chem. Phys.* **19**, 9698 (2017). doi:10.1039/C7CP00144D
- [19] M.T. Baeza-Romero, F. Gaie-Levrel, A. Mahjoub, V. López-Arza, G.A. Garcia and L. Nahon, *Eur. Phys. J. D.* **70**, 267 (2016). doi:10.1140/epjd/e2016-70463-3
- [20] D.V. Chicharro, S. Marggi Poullain, L. Banares, H.R. Hrodmarsson, G.A. Garcia and J.-C. Loison, *Phys. Chem. Chem. Phys.* **21**, 12763 (2019). doi:10.1039/C9CP02538C
- [21] K. Voronova, K.M. Ervin, K.G. Torma, P. Hemberger, A. Bodi, T. Gerber, D.L. Osborn and B. Sztáray, *J. Phys. Chem. Lett.*, 534 (2018). doi:10.1021/acs.jpcllett.7b03145
- [22] X. Tang, X. Gu, X. Lin, W. Zhang, G.A. Garcia, C. Fittschen, J.-C. Loison, K. Voronova, B. Sztáray, and L. Nahon, *J. Chem. Phys.* **152**, 104301 (2020). doi:10.1063/5.0002109.
- [23] B. Sztáray, K. Voronova, K.G. Torma, K.J. Covert, A. Bodi, P. Hemberger, T. Gerber and D.L. Osborn, *J. Chem. Phys.* **147** 013944 (2017). doi:10.1063/1.4984304
- [24] P. Oßwald, P. Hemberger, T. Bierkandt, E. Akyildiz, M. Köhler, A. Bodi, T. Gerber, and T. Kasper, *Rev. Sci. Instrum.* **85**, 025101 (2014). doi:10.1063/1.4861175.
- [25] J. Bourgalais, Z. Gouid, O. Herbinet, G.A. Garcia, P. Arnoux, Z. Wang, L.S. Tran, G. Vanhove, M. Hochlaf, L. Nahon and F. Battin-Leclerc, *Phys. Chem. Chem. Phys.* **22**, 1222 (2020). doi:10.1039/C9CP04992D
- [26] J. Pieper, S. Schmitt, C. Hemken, E. Davies, J. Wullenkord, A. Brockhinke, J. Krüger, G.A. Garcia, L. Nahon, A. Lucassen, W. Eisfeld and K. Kohse-Höinghaus, *Z. Phys. Chem.* **232**, 153 (2018). doi:10.1515/zpch-2017-1009
- [27] P. Hemberger, Z. Pan, A. Bodi, J.A. van Bokhoven, T.K. Ormond, G.B. Ellison, N. Genossar, and J.H. Baraban, *Chemphyschem* (2020). doi:10.1002/cphc.202000477.
- [28] P. Hemberger, A.J. Trevitt, T. Gerber, E. Ross and G. da Silva, *J. Phys. Chem. A.* **118**, 3593 (2014). doi:10.1021/jp501117n
- [29] P. Hemberger, J.A. van Bokhoven, J. Pérez-Ramírez and A. Bodi, *Catal. Sci. Technol.* **10**, 1975 (2020). doi:10.1039/C9CY02587A
- [30] G.A. Garcia, B.K.C. de Miranda, M. Tia, S. Daly, and L. Nahon, *Rev. Sci. Instrum.* **84**, 053112 (2013). doi:10.1063/1.4807751.

- [31] A. Bodi, P. Hemberger, T. Gerber and B. Sztaray, *Rev. Sci. Instrum.* **83** 083105 (2012). doi:10.1063/1.4742769
- [32] L. Nahon, N. de Oliveira, G.A. Garcia, J.-F. Gil, B. Pilette, O. Marcouillé, B. Lagarde and F. Polack, *J. Synchrotron Rad.* **19**, 508 (2012). doi:10.1107/S0909049512010588
- [33] M. Johnson, A. Bodi, L. Schulz and T. Gerber, *Nucl. Instrum. Meth. A.* **610**, 597 (2009). doi:10.1016/j.nima.2009.08.069
- [34] X. Tang, G.A. Garcia, J.-F. Gil, and L. Nahon, *Rev. Sci. Instrum.* **86**, 123108 (2015). doi:10.1063/1.4937624
- [35] G.A. Garcia, X. Tang, J.-F. Gil, L. Nahon, M. Ward, S. Batut, C. Fittschen, C.A. Taatjes, D.L. Osborn, and J.-C. Loison, *J. Chem. Phys.* **142**, 164201 (2015). doi:10.1063/1.4918634
- [36] Y. Bedjanian, *J. Phys. Chem. A.* **122**, 3156 (2018). doi:10.1021/acs.jpca.8b01371
- [37] B. Mercier, M. Compin, C. Prevost, G. Bellec, R. Thissen, O. Dutuit and L. Nahon, *J. Vac. Sci. Technol. A.* **18**, 2533 (2000). doi:10.1116/1.1288196
- [38] A.T.J.B. Eppink and D.H. Parker, *Rev. Sci. Instrum.* **68**, 3477 (1997). doi:10.1063/1.1148310
- [39] G.A. Garcia, L. Nahon and I. Powis, *Rev. Sci. Instrum.* **75**, 4989 (2004). doi:10.1063/1.1807578
- [40] L. Minnhagen, *J. Opt. Soc. Am.* **63**, 1185 (1973). doi:10.1364/JOSA.63.001185
- [41] C.E. Moore, *Tables of Spectra of Hydrogen, Carbon, Nitrogen, and Oxygen Atoms and Ions* (CRC Press, 1993).
- [42] S. G. Lias, in *NIST Chemistry WebBook*, NIST Standard Reference Database 69, P. J. Linstrom and W. G. Mallard (Eds), National Institute of Standards and Technology, GaithersburgMD, 2020, 20899 pp.
- [43] Y. Shao, Z. Gan, E. Epifanovsky, A.T.B. Gilbert, M. Wormit, J. Kussmann, A.W. Lange, A. Behn, J. Deng, X. Feng, D. Ghosh, M. Goldey, P.R. Horn, L.D. Jacobson, I. Kaliman, R.Z. Khaliullin, T. Ku \approx δ , A. Landau, J. Liu, E.I. Proynov, Y.M. Rhee, R.M. Richard, M.A. Rohrdanz, R.P. Steele, E.J. Sundstrom, H.L. Woodcock, P.M. Zimmerman, D. Zuev, B. Albrecht, E. Alguire, B. Austin, G.J.O. Beran, Y.A. Bernard, E. Berquist, K. Brandhorst, K.B. Bravaya, S.T. Brown, D. Casanova, C.-M. Chang, Y. Chen, S.H. Chien, K.D. Closser, D.L. Crittenden, M. Didenhofen, R.A. DiStasio, H. Do, A.D. Dutoi, R.G. Edgar, S. Fatehi, L. Fusti-Molnar, A. Ghysels, A. Golubeva-Zadorozhnaya, J. Gomes, M.W.D. Hanson-Heine, P.H.P. Harbach, A.W. Hauser, E.G. Hohenstein, Z.C. Holden, T.-C. Jagau, H. Ji, B. Kaduk, K. Khistyayev, J. Kim, J. Kim, R.A. King, P. Klunzinger, D. Kosenkov, T. Kowalczyk, C.M. Krauter, K.U. Lao, A.D. Laurent, K.V. Lawler, S.V. Levchenko, C.Y. Lin, F. Liu, E. Livshits, R.C. Lochan, A. Luenser, P. Manohar, S.F. Manzer, S.-P. Mao, N. Mardirossian, A.V. Marenich, S.A. Maurer, N.J. Mayhall, E. Neuscamman, C.M. Oana, R. Olivares-Amaya, D.P.O. \AA Neill, J.A. Parkhill, T.M. Perrine, R. Peverati, A. Prociuk, D.R. Rehn, E. Rosta, N.J. Russ, S.M. Sharada, S. Sharma, D.W. Small, A. Sodt, et al., *Mol. Phys.* **113**, 184 (2015). doi:10.1080/00268976.2014.952696
- [44] M.J. Frisch, G.W. Trucks, H.B. Schlegel, G.E. Scuseria, M.A. Robb, J.R. Cheeseman, G. Scalmani, V. Barone, G.A. Petersson, H. Nakatsuji, X. Li, M. Caricato, A.V. Marenich, J. Bloino, B.G. Janesko, R. Gomperts, B. Men- nucci, H.P. Hratchian, J.V. Ortiz, A.F. Izmaylov, J.L. Sonnenberg, Williams F. Ding, F. Lipparini, F. Egidi, J. Goings, B. Peng, A. Petrone, T. Henderson, D. Ranasinghe, V.G. Zakrzewski, J. Gao, N. Rega, G. Zheng, W. Liang, M. Hada, M. Ehara, K. Toyota, R. Fukuda, J. Hasegawa, M. Ishida, T. Nakajima, Y. Honda, O. Kitao, H. Nakai, T. Vreven, K. Throssell, J.A. Montgomery Jr, J.E. Peralta, F. Ogliaro, M.J. Bearpark, J.J. Heyd, E.N. Brothers, K.N. Kudin, V.N. Staroverov, T.A. Keith, R. Kobayashi, J. Normand, K. Raghavachari, A.P. Rendell, J.C. Burant, S.S. Iyengar, J. Tomasi, M. Cossi, J.M. Millam, M. Klene, C. Adamo, R. Cammi, J.W. Ochterski, R.L. Martin, K. Morokuma, O. Farkas, J.B. Foresman, and D.J. Fox, *Gaussian 16, Revision A.03* (Gaussian, Inc., Wallingford, CT, 2016).
- [45] J.M.L. Martin and G. de Oliveira, *J. Chem. Phys.* **111**, 1843 (1999). doi:10.1063/1.479454
- [46] E.C. Barnes, G.A. Petersson, J.A. Montgomery, M.J. Frisch and J.M.L. Martin, *J. Chem. Theory Comput.* **5**, 2687 (2009). doi:10.1021/ct900260g
- [47] J.C. Pouilly, J.P. Schermann, N. Nieuwjaer, F. Lecomte, G. Gregoire, C. Desfrancois, G.A. Garcia, L. Nahon, D. Nandi, L. Poisson and M. Hochlaf, *Phys. Chem. Chem. Phys.* **12**, 3566 (2010). doi:10.1039/b923630a
- [48] C.M. Gabrys, D. Uy, M.-F. Jagod, T. Oka and T. Amano, *J. Phys. Chem.* **99**, 15611 (1995). doi:10.1021/j100042a042
- [49] M. Bogey, H. Bolvin, M. Cordonnier, C. Demuynck, J.L. Destombes, R. Escribano and P.C. Gomez, *Can. J. Phys.* **72**, 967 (1994). doi:10.1139/p94-127
- [50] C. Demuynck, *J. Mol. Spectrosc.* **168**, 215 (1994). doi:10.1006/jmsp.1994.1272
- [51] Z. Vager, D. Zajfman, T. Graber and E.P. Kanter, *Phys. Rev. Lett.* **71**, 4319 (1993). doi:10.1103/PhysRevLett.71.4319
- [52] M.W. Crofton, M. Jagod, B.D. Rehfuss and T. Oka, *J. Chem. Phys.* **91**, 5139 (1989). doi:10.1063/1.457612
- [53] E.P. Kanter, Z. Vager, G. Both and D. Zajfman, *J. Chem. Phys.* **85**, 7487 (1986). doi:10.1063/1.451338
- [54] P.C. Varras, M.G. Siskos, and P.S. Gritzapis, *Mol. Phys.* **118** (14), e1706778 (2020). doi:10.1080/00268976.2019.1706778.
- [55] B.T. Psciuk, V.A. Benderskii and H.B. Schlegel, *Theor. Chem. Acc.* **118**, 75 (2007). doi:10.1007/s00214-006-0242-x
- [56] A.R. Sharma, J. Wu, B.J. Braams, S. Carter, R. Schneider, B. Shepler, and J.M. Bowman, *J. Chem. Phys.* **125**, 224306 (2006). doi:10.1063/1.2402169.
- [57] H.R. Hrodmarsson, G.A. Garcia, L. Nahon, J.-C. Loison and B. Gans, *Phys. Chem. Chem. Phys.* **21** 25907 (2019). doi:10.1039/C9CP05809E
- [58] O.J. Harper, S. Boyé-Péronne, G.A. Garcia, H.R. Hrodmarsson, J.-C. Loison, and B. Gans, *J. Chem. Phys.* **152**, 041105 (2020). doi:10.1063/1.5139309.
- [59] F. Merkt, O.A.R. Seiler, R. Signorel, H. Palm, H. Schmutz and R. Gunzinger, *J. Phys. B.* **31**, 1705 (1998). doi:10.1088/0953-4075/31/8/020
- [60] J.W. Brault, *Mikrochim. Acta.* **93**, 215 (1987). doi:10.1007/BF01201691